Engineering Fracture Mechanics Vol. 32, No. 3, pp. 361–377, 1989
Printed in Great Britain.

0013-7944/89 $3.00 + 0.00

FATIGUE CRACK PROPAGATION IN ARALL® LAMINATES: MEASUREMENT OF THE EFFECT OF CRACK-TIP SHIELDING FROM CRACK BRIDGING

R. O. RITCHIE,† WEIKANG YU† and R. J. BUCCI‡

†Department of Materials Science and Mineral Engineering, University of California, Berkeley, CA 94720, U.S.A. ‡Alcoa Laboratories, Alcoa Center, PA 15069, U.S.A.

Abstract—Fatigue crack propagation behavior has been examined in a 2024-T3 aluminum alloy/aramid-fiber epoxy 3/2 laminated composite, ARALL®-2 LAMINATE, with the objective of quantitatively evaluating the primary mechanisms of crack-tip shielding. Based on metallographic and crack-path sectioning and *in situ* compliance measurements, it is confirmed that the vastly superior (longitudinal) fatigue crack growth resistance of the laminate is primarily associated with extensive crack bridging from unbroken aramid fibers in the wake of the crack, with a smaller contribution from crack closure due to the wedging of fracture-surface asperities. The bridging phenomenon, which results in a *local* (near-tip) reduction in the maximum stress intensity (K_{max}) in the cycle, is shown to rely on controlled delamination, created by weak interfacial bonding between fibers and the epoxy matrix, which acts to limit fiber breakage. By progressively removing material from the crack wake, the length of the "bridging zone" behind the crack tip is found to be as large as 3–5 mm. Using a novel compliance-measurement scheme to evaluate the local reduction in K_{max} from bridging and the local increase in K_{min} from closure, an effective stress-intensity range (ΔK_{eff}), experienced at the crack tip, is estimated and shown to provide excellent agreement in normalizing seemingly non-unique crack propagation data presented in the literature in terms of the nominal (applied) stress intensity (ΔK).

INTRODUCTION

ARAMID-fiber reinforced aluminum-alloy laminates (ARALL® LAMINATE) are a new class of hybrid materials which consist of alternating layers of thin aluminum-alloy sheets bonded by a structural metal adhesive impregnated with high-strength unidirectional aramid fibers (Fig. 1). Originally developed for fatigue-critical aircraft structures where up to 50% potential weight saving has been predicted[1–4], these composites show a range of attractive, albeit directional, properties, including 15–20% lower density, up to 60% higher strength (at comparable stiffness), good impact and damping properties, and most importantly superior fatigue crack propagation resistance, compared to monolithic high-strength aluminum alloys[1–5]. Moreover, property characteristics can be readily modified, for example, through the use of post-stretching or by using various matrix alloys, varying fiber-resin systems, and different stacking sequences and cross-plies, although few of these variants are commercially available at present.

ARALL derives its superior crack-growth properties (under tensile loading) by promoting extensive crack bridging in the wake of the crack tip[4–8]. Mechanistically, for crack extension perpendicular to the fiber direction, as the crack propagates in the aluminum layers, controlled delamination between the metal, epoxy and fiber interfaces redistributes stresses both ahead and behind the tip, permitting individual aramid fibers to remain intact and span the crack in the wake of the tip[7, 8]. Thus, similar to behavior in certain ceramic–matrix composites[9], the fibers act as bridges to restrain crack opening, thereby reducing the effective "crack driving force" actually experienced at the crack tip. In stretched ARALL Laminates, where the metal layers are left in residual compression and the fibers in residual tension, self-arrest can result with crack extension[10], leading to the claim that ARALL is a "fatigue insensitive" material.

Crack bridging in ARALL Laminates is an example of crack-tip shielding, where toughness is enhanced, or more generally crack advance is impeded, not by increasing the intrinsic microstructural resistance but by mechanisms which act to lower the *local* near-tip "driving force"[11, 12]. As illustrated schematically in Fig. 2[11, 12], other examples include rubber-toughening in polymers[13], transformation, microcrack and fiber toughening in ceramics[14, 15],

®ARALL LAMINATE is a registered trademark of the Aluminum Company of America.

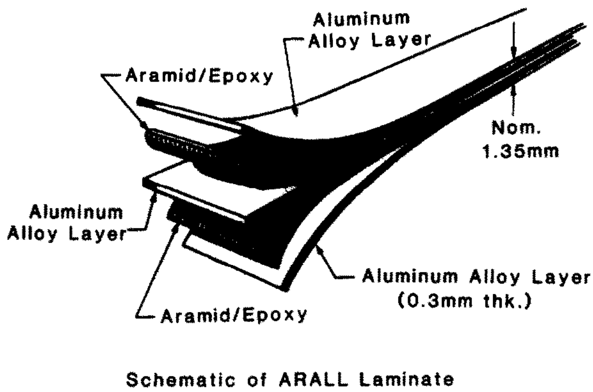

Fig. 1. Illustration of the lay-up of 3/2 ARALL-2 Laminate.

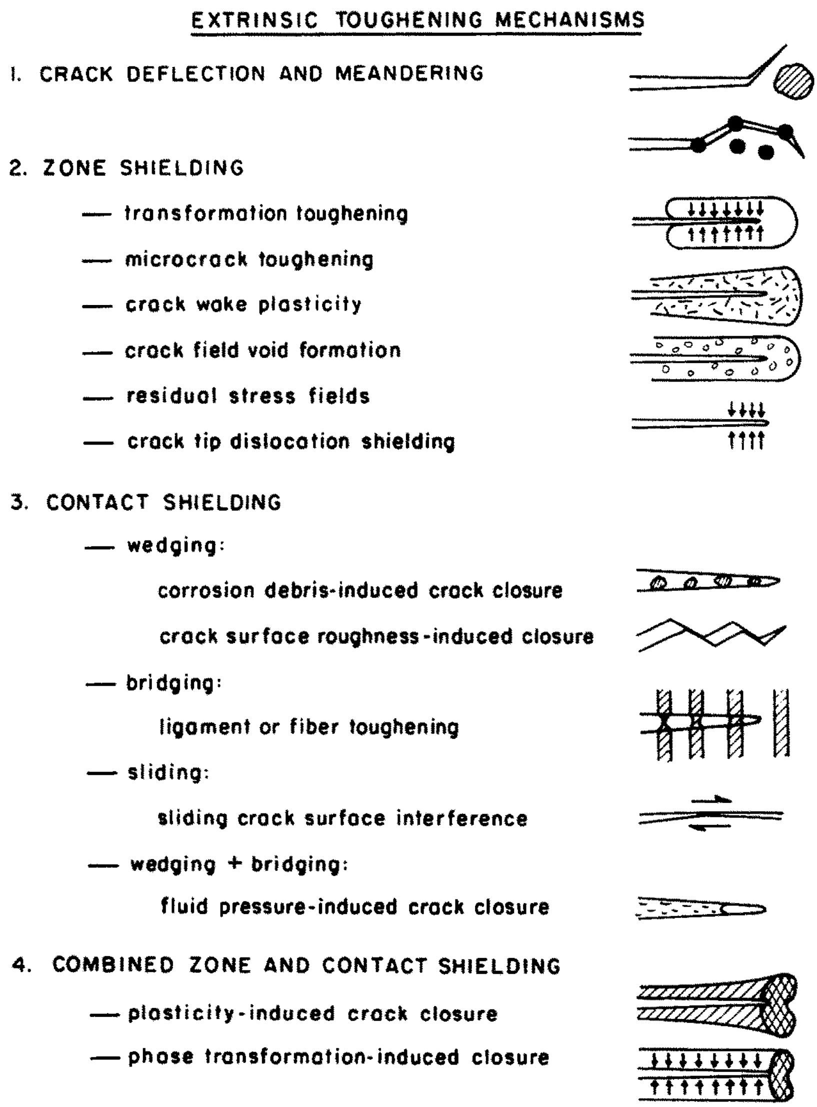

Fig. 2. Schematic representation of the classes and mechanisms of crack-tip shielding[11, 12].

crack bridging via uncracked ligaments in metals, ceramics and composites[16–18], and crack closure in fatigue[12, 19]. In all these cases, the predominant shielding mechanisms act in the crack wake such that, depending upon the extent of the "shielding zone" behind the tip, crack-growth behavior becomes crack-size dependent, i.e. in terms of the globally calculated applied stress intensity K, the usually assumed similitude of the crack-tip fields for cracks of differing size will be compromised. This leads to certain definitive fracture properties, such as marked resistance-curve toughness behavior, as seen for example in toughened ceramics[14, 15, 17], and the elevated growth rates of small cracks, as seen for near-threshold fatigue in metals[11, 20, 21].

The theoretical modelling of crack-tip shielding is in many cases well developed, particularly for the transformation/microcrack toughening[14, 15, 22] and crack-bridging mechanisms [7–9, 16, 17]. There have been few studies, however, to verify experimentally these models and specifically to measure the extent of shielding and the effective near-tip "driving force". An exception to this is crack closure in fatigue where an effective stress-intensity range can be evaluated, for example, in terms of compliance changes resulting from physical contact between the crack surfaces during the unloading cycle (e.g. refs [11, 23, 24]). The primary objective of the present work is to describe experimental techniques to measure quantitatively the magnitude of crack-tip shielding by crack bridging as well as crack closure in an ARALL Laminate, in order to estimate the effective near-tip stress-intensity range during fatigue crack growth in this material. In addition, the mechanistic characteristics of crack propagation, delamination and crack-bridging behavior in the laminate are described for a wide spectrum of growth rates.

EXPERIMENTAL PROCEDURES

Materials

The ARALL Laminate used in this study was a 1.35-mm thick five-layer composite with two 0.2-mm thick unidirectional aramid-fiber/epoxy ("prepreg") layers sandwiched between three 0.3-mm thick chromic-acid-anodized and primed 2024-T3 aluminum-alloy sheets, supplied and designated by Alcoa as a 3/2 ARALL-2 Laminate. The prepreg layers consist of an epoxy based adhesive system impregnated with uniaxial, high-modulus aramid fibers, in a 50/50 fiber/adhesive weight ratio. The fiber direction is aligned parallel to the rolling direction of the aluminum sheet. Curing is achieved at 121°C (with no subsequent stretch)[25]. The density of the resulting material is 2.29 g/cm^3, 18% lower than 2024. For comparative purposes, ARALL-2 Laminate behavior is compared to its 2024-T351 monolithic alloy counterpart.

Microstructure and mechanical properties

The microstructure of the laminate, including an enlarged view of the prepreg layer, is shown in Fig. 3. It is apparent that the fibers are not distributed evenly throughout the adhesive layer; resin-rich (i.e. fiber-poor) regions exist near the prepreg/metal interface[7]. Typical mechanical properties for the longitudinal (0°, loading parallel to fiber direction) and transverse (90°, loading perpendicular to fiber direction) orientations are compared to monolithic 2024-T3 (1.6-mm thick sheet) in Table 1[25, 26].

Fatigue testing

Fatigue crack propagation tests on ARALL-2 Laminates were performed with compact C(T) test pieces, machined to a width of 50 mm from the full thickness of the plate in the L–T (0°, crack

Table 1. Typical mechanical properties of 3/2 ARALL-2 Laminate and 2024-T3

Average mechanical property	3/2 ARALL-2 Laminate		Monolithic 2024-T3	
	L (0°)	T (90°)	L	T
Tensile modulus of elasticity (GPa)	64.1	49.0	72.4	72.4
Ultimate tensile strength (MPa)	717	317	455	448
Tensile yield strength (MPa)	359	228	359	324
Compressive yield strength (MPa)	262	234	304	345
Tensile total strain to failure (%)	2.5	12.7	19.0	19.0

growth perpendicular to fiber direction) and T-L (90°, crack growth parallel to fiber direction) orientations. Comparison tests on 2024-T351 were performed on 7-mm thick C(T) test pieces, machined in the T–L orientation from the center thickness of 25-mm thick plate. All testing was carried out in controlled room-temperature air (22°C, 45% relative humidity) using a computer-controlled electroservo-hydraulic testing machine, operating at 50 Hz sinusoidal frequency with a load ratio ($R = K_{min}/K_{max}$) of 0.1.

Crack lengths were monitored using a direct-current electrical-potential technique on the outer aluminum layer (Fig. 4). The accuracy of this technique in thin sheet was estimated to be within ± 0.01 mm on crack length. Additionally, the compliance of the specimen was monitored using a back-face strain gauge mounted on the central aluminum layer at the midpoint opposite the crack mouth (Fig. 4). Both electrical-potential and back-face strain signals were fed into a real-time computerized data-acquisition and control system, which was used both to control the test and to compute continuously compliance and crack-closure loads (see below). Stress intensities were calculated from standard handbook solutions[27] for the compact geometry, using the full thickness of the composite (unless otherwise stated).

The crack propagation tests were performed under computer control with a constant stress-intensity gradient, in general accordance with ASTM Standard E 647-86A. Data were first generated under decreasing ΔK conditions using an automated load-shedding scheme of $\Delta K = \Delta K_0 \exp[C^* (a - a_0)]$, where ΔK and a are the instantaneous values of stress-intensity range ($K_{max} - K_{min}$) and crack length, ΔK_0 and a_0 are their initial values, and C^* is the normalized stress-intensity gradient set to -0.1 per mm of crack extension. Following crack arrest at a "threshold" condition, tests were continued under increasing ΔK conditions, with C^* set to 0.15 per mm. Using these procedures, crack propagation rate data were generated over a wide spectrum of growth rates, from roughly 10^{-11} to 10^{-5} m/cycle.

RESULTS AND DISCUSSION

Fatigue crack growth behavior

Results of the constant-amplitude fatigue crack propagation tests, in the form of growth rates, da/dN, as a function of the nominal stress-intensity range, ΔK, are shown in Fig. 5 for the 0° (L–T) and 90° (T–L) orientations in ARALL-2 Laminate; data are compared to that for monolithic 2024-T351 (T–L orientation).

Where fatigue crack propagation in the laminate is along the fiber direction (90° orientation), growth rates are faster than in the monolithic alloy, although the form of the growth-rate curve

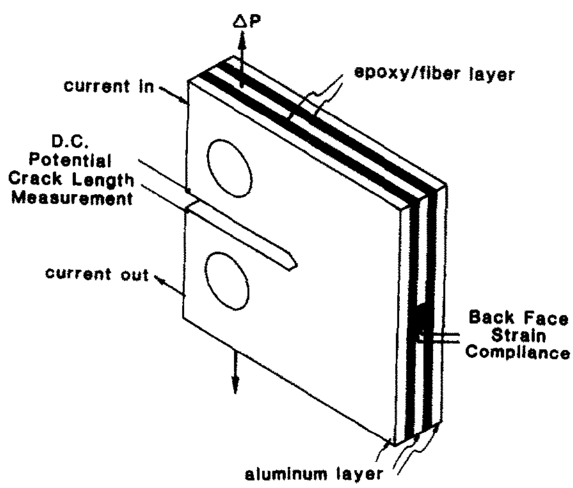

Fig. 4. Illustration of the fatigue test specimen showing the location of the electrical-potential crack monitoring probes, attached to the outer aluminum layer and the back-face strain gauge used to measure compliance, attached to the central aluminum layer.

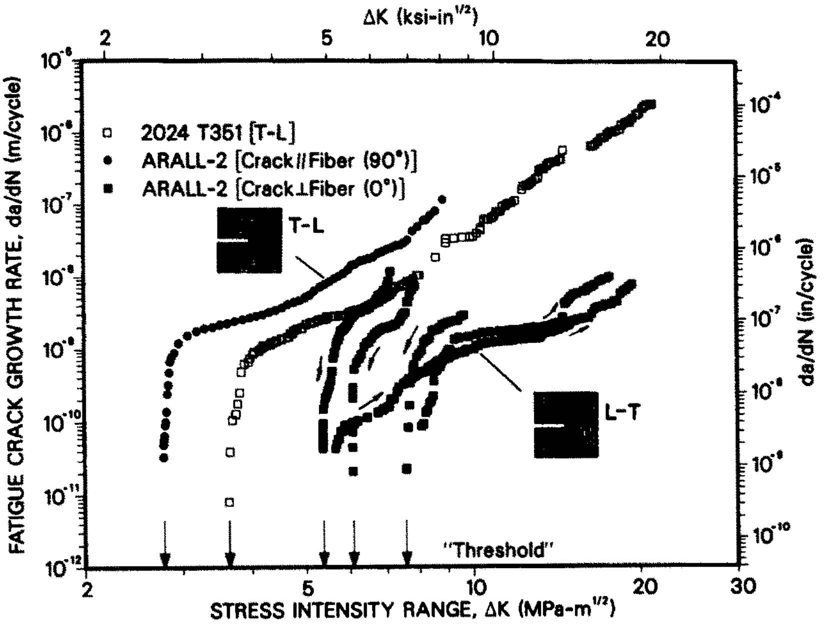

Fig. 5. Variation in fatigue crack propagation rates (da/dN) for ARALL-2 Laminate, as a function of the nominal stress-intensity range ($\Delta K = K_{max} - K_{min}$), in the longitudinal (0°, L–T) and transverse (90°, T–L) orientations. Data are compared with results for monolithic 2024-T351 alloy (T–L orientation). Vertical arrows show the effective fatigue "thresholds", i.e. the values of ΔK at crack arrest. Small arrows on curves indicate whether data were obtained under decreasing or increasing growth-rate conditions.

is similar. If the ARALL data for this orientation are normalized with respect to the actual total thickness of the aluminum in the composite, i.e. assume that the aluminum carries all load, crack growth rates for ARALL-2 (90°) coincide with those for the monolithic 2024-T351 alloy (Fig. 6). This result implies that the role of the fibers (and the resin) in the laminate can be ignored for crack growth in the transverse (90°) direction.

Conversely, where fatigue crack propagation in the laminate is perpendicular to the fiber direction (0° orientation), due to the contribution of the aramid fibers, behavior is quite different

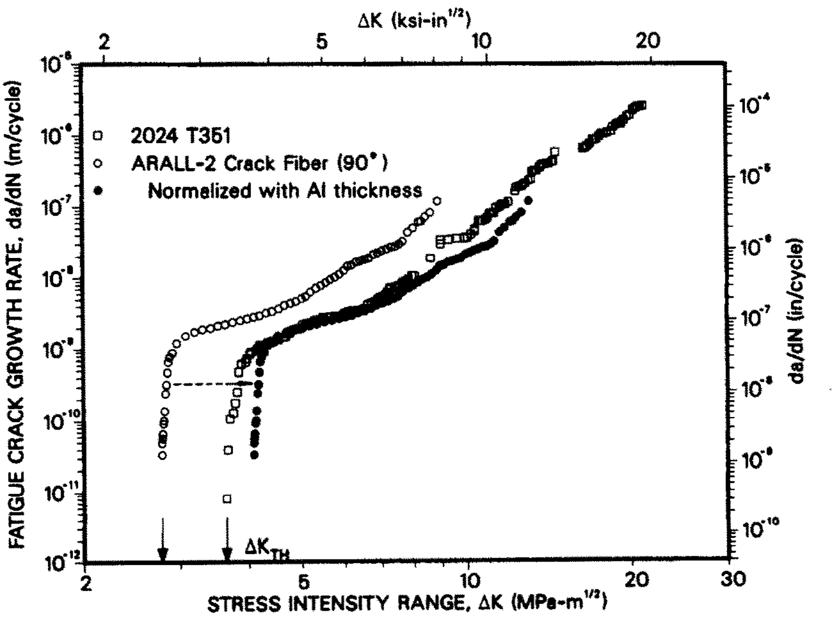

Fig. 6. Variation in fatigue crack propagation rates (da/dN) as a function of the nominal stress-intensity range (ΔK) for ARALL-2 and 2024-T351 alloy in the transverse (T–L) orientation, showing the correspondence of growth-rate behavior in the laminate and the monolithic alloy by assuming that the aluminum layers carry all the load in ARALL-2.

from 2024-T351. Firstly, growth rates in the laminate are in general significantly slower (by up to almost three orders of magnitude) than in the monolithic aluminum alloy, indicating that the fatigue crack growth resistance of ARALL-2 in this orientation is extremely high. Secondly, similar to behavior reported for other ARALL laminates[1–8, 10, 28], crack growth rates become non-unique with respect to the nominal stress-intensity range ΔK, showing a marked history and crack-size dependence.

Fractographic studies

The reinforcement role of the fibers during crack growth in the latter longitudinal (0°) orientation was examined using scanning electron microscopy of metallographic sections taken across the crack perpendicular to the crack surface. Figure 7 shows one such cross-section, located ~ 3 mm from the crack tip, looking into the crack in the crack propagation direction, i.e. from the wake toward the tip. The fatigue crack can be readily seen in the aluminum layers, but is also still visible in the epoxy layer. Numerous strands of aramid fibers, however, remain unbroken across the crack.

To lower the probability of fiber breakage necessary to permit such crack bridging, some degree of controlled delamination is essential to reduce the magnitude of fiber loading and lower through-thickness constraint[8]. Claims that such delamination occurs principally within the epoxy near the prepreg/metal interface, specifically at the boundary between the fiber-rich and resin-rich layers[6–8], have been made. However, the fact that the crack can be imaged throughout the thickness of the epoxy layer (Figs 7 and 8) suggests an alternative explanation. In the present case, the interface between the aluminum sheet and the epoxy, and between the resin-rich and fiber-rich layers within the epoxy, only suffered minor delamination, whereas extensive separation was apparent among various bundles of fibers, implying that failure of individual fiber/epoxy interfaces is the primary source of the delamination process.

Figure 7 also shows evidence of "bulged out" fibers at the crack line, which suggests some degree of prior kinking. Fiber kinking is known to be severely detrimental to the fatigue properties of ARALL as it promotes breakage of the aramid fibers[28]; for this reason ARALL laminates are intended for tension-dominated cyclic loading application and as such are not suited for high compressive loading during service. However, such kinking in the present study is probably the result of the predominantly bending stress field implicit with compact test piece which, unlike center-cracked tension geometries, subjects fibers located well ahead of the crack tip (below the neutral axis) to prior compressive loads. Crack growth behavior in ARALL is thus predicted to be geometry-dependent.

Another example of geometry-dependent behavior is apparent at high stress-intensity ranges, where the marked difference in crack propagation resistance between the 0° and 90° orientations (due to selective fiber bridging) leads to a tendency for crack growth in the 0° direction to deviate along the fiber direction in compact C(T) geometries. This phenomenon causes marked crack bifurcation, as shown in Fig. 8, which results in additional crack-tip shielding by crack deflection at high ΔK. However, in center-cracked tension CC(T) sheet geometries, where off-angle crack propagation is not stabilized, such crack-bifurcation behavior is rarely observed.

Measurement of crack-bridging zone

In order to verify further the role of fiber bridging influencing fatigue crack propagation behavior in ARALL, and specifically to determine the location and size of the "bridging zone" of unbroken fibers behind the crack tip (Fig. 9), experiments were performed where the wake of the crack was progressively removed while simultaneously monitoring the change in elastic compliance (as a measure of how much the fibers restrain crack opening).

The experiment was conducted on an arrested crack that had been cycled for 10^7 cycles at an apparent threshold of $\Delta K = 7.6\ \mathrm{MPa}\sqrt{m}$, following normal load-shedding procedures. Using a fine jeweller's saw, a 1-mm wide slot was machined from the V-notch along the dormant crack to within ~ 0.2 mm of the crack tip. Approximately every 1 mm, the elastic compliance was measured using the back-face strain gauge mounted on the central aluminum layer (Fig. 4), while monitoring the length ($\tilde{a}$) of the remaining portion of the crack with a travelling microscope; results are plotted in Fig. 10(a). For the ~ 26-mm long crack, removing the wake to within roughly 5 mm of the crack

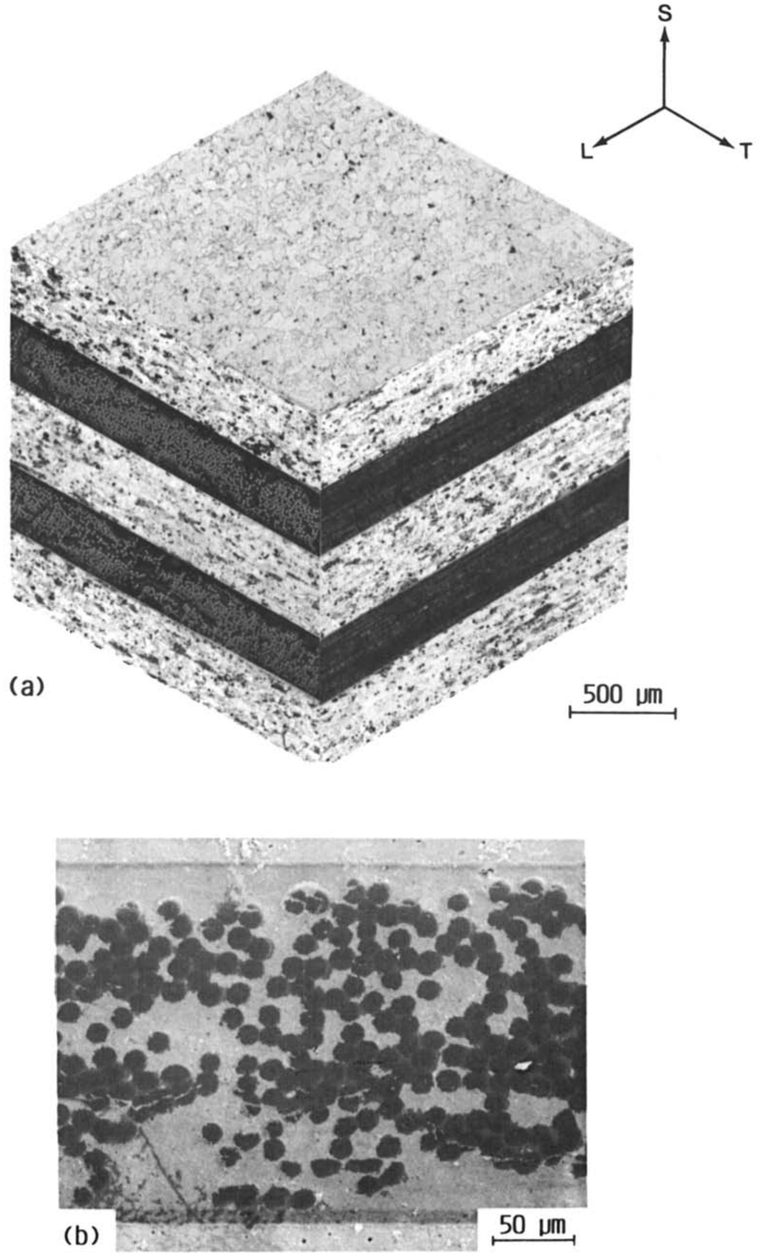

Fig. 3. Optical micrographs of (a) three-dimensional microstructure of ARALL-2, and (b) cross-section showing prepreg layers sandwiched between aluminum layers. Note in (b) the resin-rich (fiber-poor) regions close to the prepreg/aluminum interfaces.

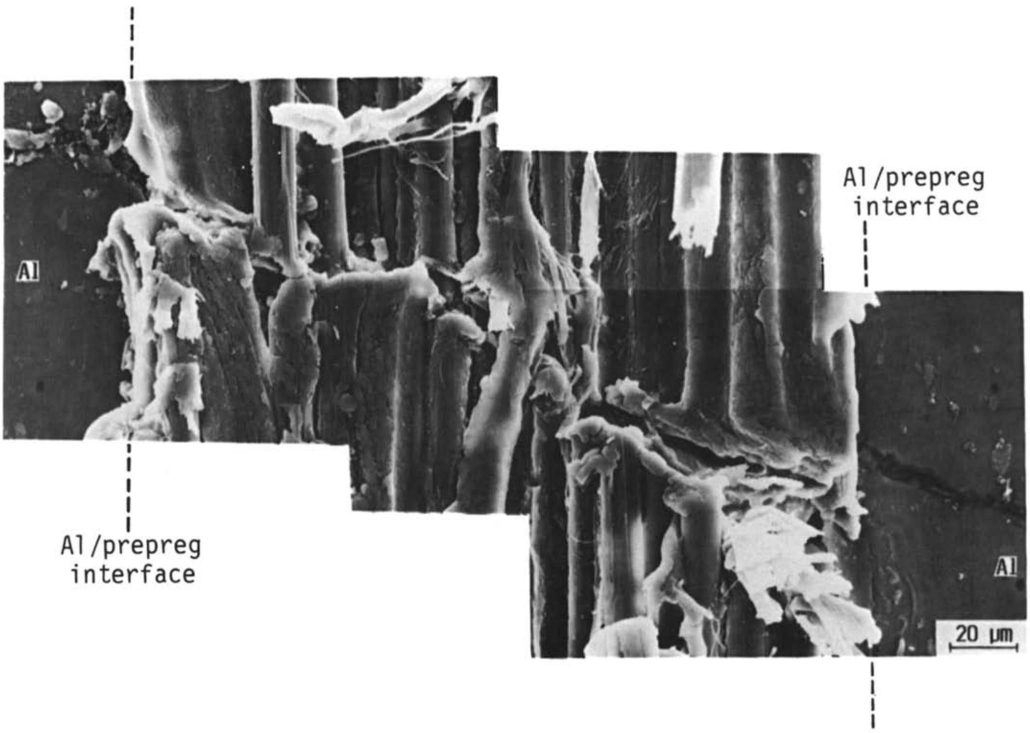

Fig. 7. Scanning electron micrograph of a metallographic section taken across the wake of a fatigue crack in ARALL-2 (imaged ~ 3 mm from the crack tip, looking into the crack mouth toward the tip), showing numerous strands of unbroken aramid fibers bridging the crack. Note that the crack is still visible in the epoxy layer, indicating that the delamination is primarily at individual fiber/epoxy interfaces.

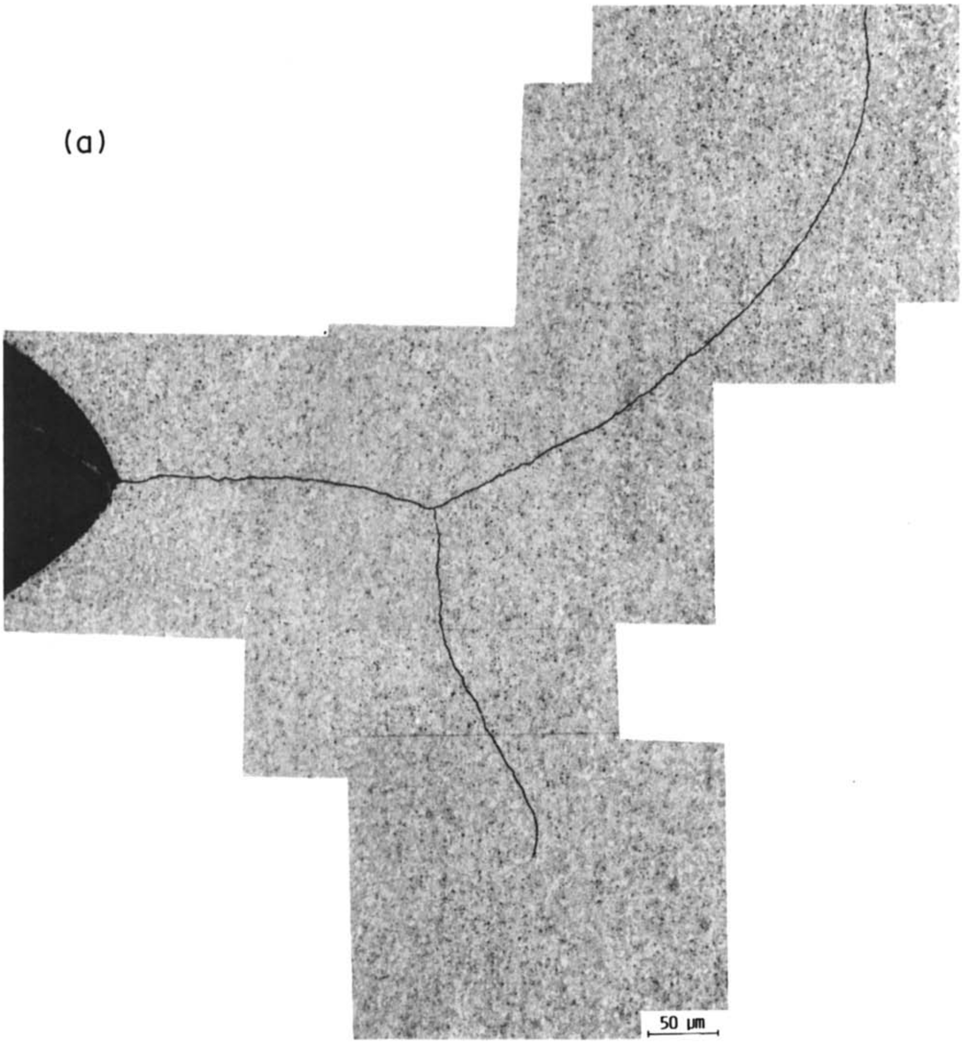

Fig. 8(a).

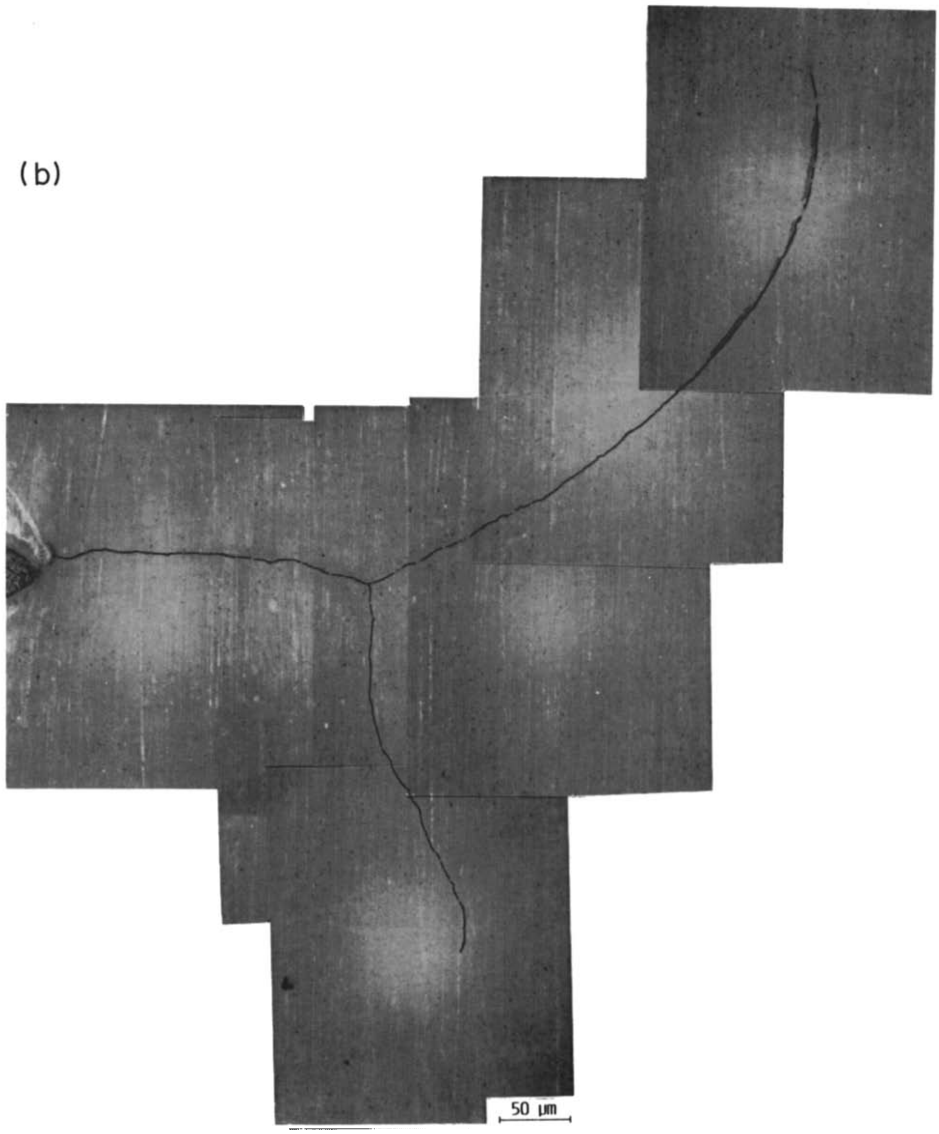

Fig. 8. Metallographic section perpendicular to the crack plane showing crack bifurcation during fatigue crack propagation at high stress-intensity ranges ($\Delta K \sim 15\ \mathrm{MPa}\sqrt{m}$) in ARALL-2, as imaged (a) in the outer aluminum layer and (b) in the epoxy layer after etching away the aluminum. Note that as the crack is still visible within the epoxy layer, the principal delamination is not at the resin-rich/fiber-rich boundary.

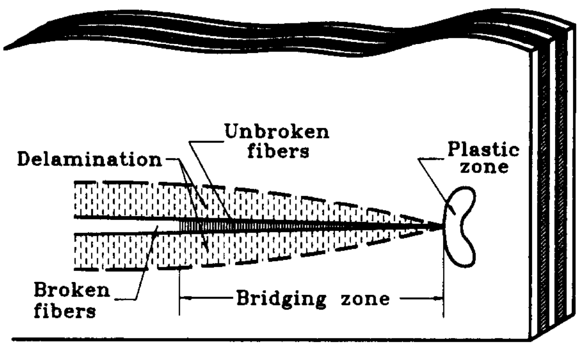

Fig. 9. Schematic illustration of a fatigue crack in ARALL, showing the location of the bridging (or shielding) zone.

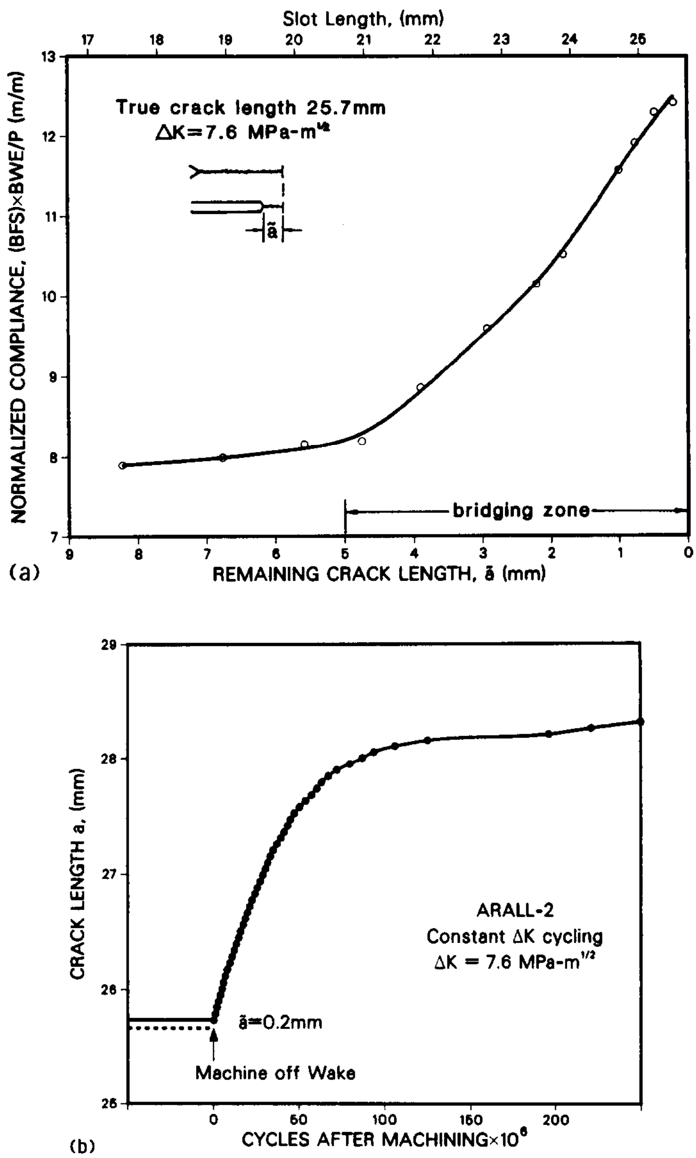

Fig. 10. Results of experiments to estimate the size of the bridging zone in ARALL showing (a) the change in compliance as a function of the remaining length of fatigue crack, $\tilde{a}$, during progressive removal of the crack wake, and (b) the initial acceleration and subsequent progressive deceleration of crack growth from the machined slot (initial $\tilde{a}$ = 0.2 mm). All results were determined at a constant ΔK of 7.6 MPa$\sqrt{m}$, where prior to machining the crack had arrested.

tip had little effect on the compliance, implying that the fibers were broken this far from the tip. Conversely, the compliance increased sharply as the last ~ 5 mm of wake were removed, indicating that the fibers in this region were originally intact across the fatigue crack and were being severed by the jeweller's saw.

Such measurements suggest a shielding (or bridging) zone in ARALL of the order of 5 mm behind the crack tip where the principal fiber bridging takes place. Compared to the size of this zone for other mechanisms of shielding in Fig. 2, this is extremely large. For example, similar wake-machining experiments in monolithic aluminum alloys to determine the extent of crack closure (primarily from asperity wedging) in the wake of arrested cracks suggest shielding-zone sizes closer to 500 μm[29, 30]. Furthermore, in the case of corrosion-debris induced crack closure, where the fretting oxide deposits accumulate only very close to the tip[31, 32], the shielding zone may be less than $\sim 10\ \mu$m. Since the magnitude of the shielding zone behind the crack tip primarily dictates the history- and crack-size dependence of the crack-growth behavior, such results are consistent with the experimental observations (Fig. 5) that longitudinal growth rates in ARALL do not display a unique dependence upon ΔK.

To examine the re-generation of the bridging zone with crack extension, following wake machining the remaining 0.2-mm fatigue crack, emanating from the machined slot, was cycled at the original "threshold" ΔK level of 7.6 MPa$\sqrt{m}$. As shown in Fig. 10(b), although the crack commenced to propagate immediately on application of the cyclic load, growth rates progressively decayed with subsequent crack extension (at constant ΔK) until the crack re-arrested after more than 10^8 cycles. The crack length needed for re-arrest, i.e. to reestablish a bridging zone behind the crack tip, can be seen to be of order of 3 mm, somewhat less than the 5 mm or so required for arrest during load shedding (Fig. 10a). Such differences presumably reflect different loading histories prior to arrest, namely decreasing ΔK conditions during programmed load shedding compared to constant ΔK conditions (at the lowest "threshold" level) in the above experiment.

Measurement of crack-tip shielding

Whereas the fatigue crack propagation properties of ARALL Laminates in the longitudinal (0°) orientation are clearly excellent, from the perspective of analysis and prediction of crack extension and lifetime, the non-uniqueness of the crack growth data (in terms of ΔK) is far from ideal. As noted above, such non-uniqueness, with respect to crack size, geometry and loading history, results from differing degrees of crack bridging in the wake of the crack (and associated delamination), which reduces the effective ΔK experienced locally at the crack tip. Although modelled by Marissen[7, 8] for the center-cracked tension geometry, there have been no attempts experimentally to measure the bridging effect, in order to determine an effective ΔK which would suitably characterize the crack-tip fields in ARALL and thus potentially normalize the longitudinal crack growth data. Below we describe an experimental scheme, intended to provide this characterization through the measurement of the effect of crack-tip shielding from both crack bridging and crack closure using combined electrical-potential and compliance monitoring.

Principle. The principle of the measurement technique is illustrated schematically in Fig. 11. Shielding is assumed to affect the applied "crack driving force", $\Delta K = K_{max} - K_{min}$, in two ways, specifically by crack closure (i.e. wedging through crack-surface contact), which primarily increases the effective K_{min}, and crack bridging, which primarily decreases the effective K_{max}.† Accordingly, the effective stress-intensity experienced at the tip may be defined as:

$$\Delta K_{eff} = K_{br} - K_{cl}, \tag{1}$$

where K_{br} is the effective K_{max} (corrected for crack bridging) and K_{cl} is the effective K_{min} (corrected for crack closure). Experimental techniques to measure each parameter are described below.

Crack closure. In aluminum alloys at low ΔK levels, the principal source of crack closure arises from wedging of crack surfaces by fracture-surface asperities (roughness-induced closure), aided

†It should be noted here that in the general case, crack closure, induced by cyclic plasticity[23] or fluid pressure[33] for example, may have a small additional influence in reducing the effective K_{max}. By the same token, depending upon the mechanical properties of the fibers, crack bridging may influence the effective K_{min}. However, the proposed measurements are not specific to the microstructural origins of the shielding mechanisms and will thus evaluate the total effect.

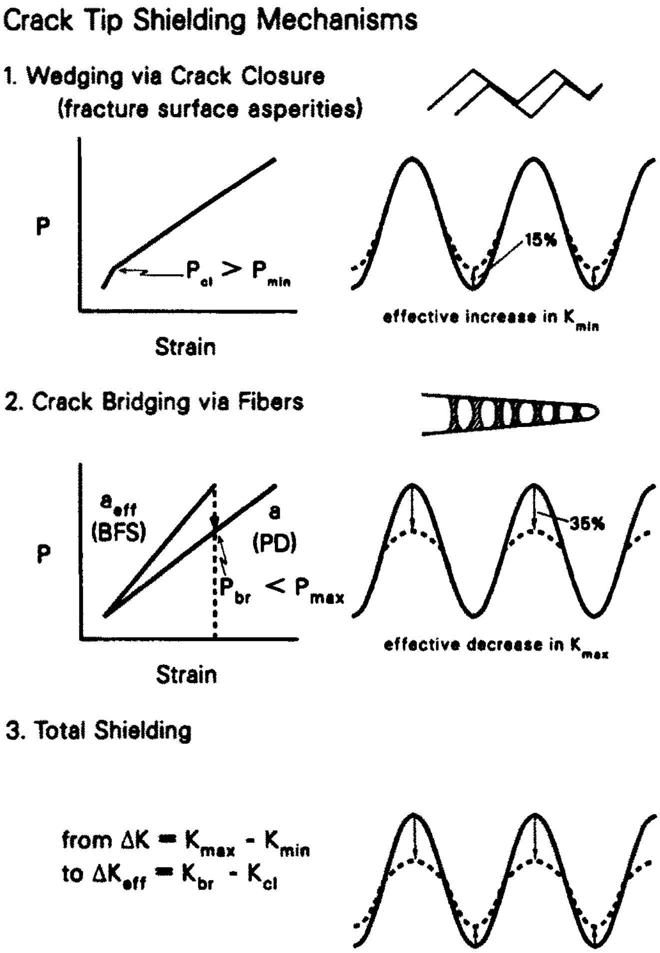

Fig. 11. Schematic illustrations of the primary crack-tip shielding mechanisms in ARALL, namely crack bridging and crack closure, and the experimental techniques used to quantify their effect on the effective near-tip "crack-driving force", i.e. $\Delta K_{eff} = K_{br} - K_{cl}$.

by that induced by cyclic plasticity in the wake of the crack tip (e.g. refs [30, 34]). Accordingly, the closure stress intensity K_{cl} is generally measured at the point of first contact of the crack surfaces during an unloading cycle (e.g. refs [11, 24]). In the present study, this was achieved by monitoring the elastic unloading compliance derived from the back-face strain gauge. Specifically, the data-acquisition and control system was programmed to determine, using a maximum correlation-coefficient procedure[11], the K_{cl} value in real time in terms of the highest load where the elastic unloading compliance curve deviated from linearity (Fig. 11).

Using such procedures, closure levels in ARALL were found to be comparable with those in monolithic 2024-T351 sheet, but due to the higher ΔK levels required for propagation, their effect was proportionally smaller. In fact, closure was clearly of secondary importance to crack bridging in governing the value of ΔK_{eff} (see below). Specifically, closure levels were enhanced with decreasing ΔK, as wedging is more effective at smaller crack opening displacements (CODs), but never resulted in more than a 15% increase in the effective K_{min}.

Crack bridging. The effect of crack bridging on the effective K_{max} value was estimated using a new technique which combines measurement of the actual length of the full crack, using electrical-potential methods on the outer aluminum layer, with measurements of the compliance of the bridged crack, using back-face strain gauges on the central aluminum layer (Fig. 4).

For each cycle, an elastic compliance curve of measured back-face strain vs load P was determined; the slope of this curve (ignoring non-linearities due to closure at very low loads) represents the compliance of the bridged crack. Simultaneously, electrical-potential measurements

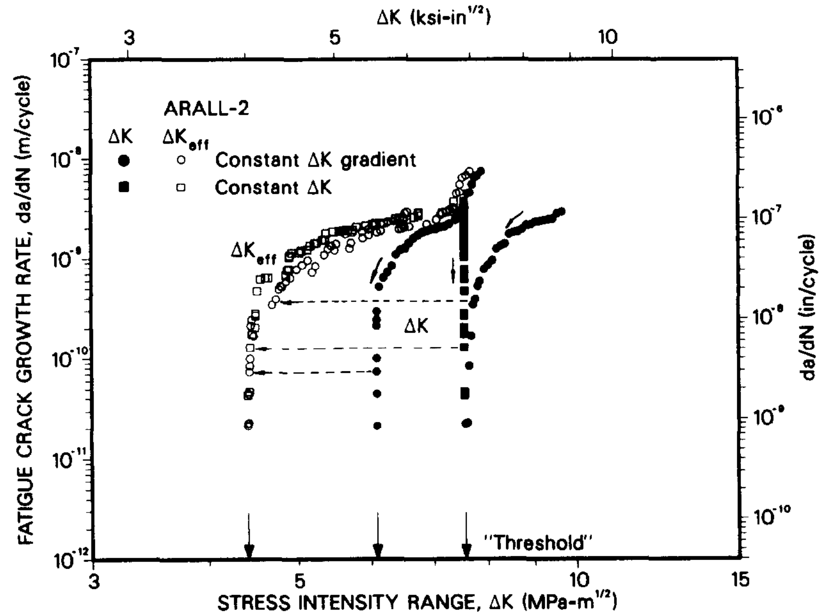

Fig. 12. Fatigue crack propagation results for ARALL-2 in the longitudinal (0°) orientation (from Figs 5 and 10), plotted as a function of the nominal ($\Delta K = K_{max} - K_{min}$) and effective ($\Delta K_{eff} = K_{br} - K_{cl}$) stress-intensity ranges. Note how characterization in terms of ΔK_{eff} normalizes the previous crack-size and history dependent growth-rate data (horizontal dashed arrows). Small arrows on curves indicate whether data were obtained under decreasing or increasing growth-rate conditions.

were used to estimate the true length of the crack and, using an experimentally verified compliance calibration for back-face strain in the C(T) geometry[35–37], the theoretical compliance curve for the full-length (unbridged) crack was computed. As illustrated in Fig. 11, the slopes of these two curves are different. The experimental curve, derived from back-face strain measurements, is steeper (implying a smaller effective crack size) because the compliance is reduced by the fiber bridges; the theoretical curve, computed from electrical measurements of the true crack length, conversely is insensitive to the bridging effect.† Thus, at a given load, the measured strain (representative of the actual crack opening displacement) can be seen to be less than that predicted from the true (unbridged) crack length, because of the restraint on crack opening by the unbroken fibers. On this basis, the reduction in effective K_{max} due to bridging can be estimated by comparing these two curves at a given strain, for example, representative of the actual COD at maximum load. As shown in Fig. 11, the measured load (P_{max}) acting on the bridged crack length is clearly larger than that predicted (P_{br}) for the true (unbridged) crack length; the difference is essentially the load carried by the bridges. Accordingly, values of P_{br} can be used to compute the approximate magnitude of K_{br} as the effective maximum stress intensity in the fatigue cycle (after correcting for bridging).

With such procedures, the measured effect of crack bridging in ARALL was found to be far greater than that due to crack closure, resulting in up to 35% reductions in effective K_{max} values in the fatigue cycle. The success of this approach may be judged with reference to Fig. 12 where, by using both closure and bridging corrections for shielding to compute ΔK_{eff} values from eq. (1), the fatigue crack propagation data for ARALL-2 in the longitudinal (0°) orientation from Fig. 5, and from Fig. 10(b) for crack growth at constant ΔK from the wake-machined notch, are replotted in terms of ΔK_{eff}. Once the allowance is made for both closure and bridging in the computation of the appropriate "crack driving force", crack propagation behavior in the laminate is no longer dependent upon history and crack size, and is a unique function of ΔK_{eff}. (Results at the highest

†In ARALL Laminates, the fiber bridges are non-conducting and thus do not compromise the electrical-potential measurements of true crack size. In materials where the bridges are conducting, or conversely where the matrix is non-conducting, actual crack size measurements can still made by monitoring the electrical resistance of a thin metal film, either evaporated or affixed to the side face of the specimen (e.g. refs [38, 39]).

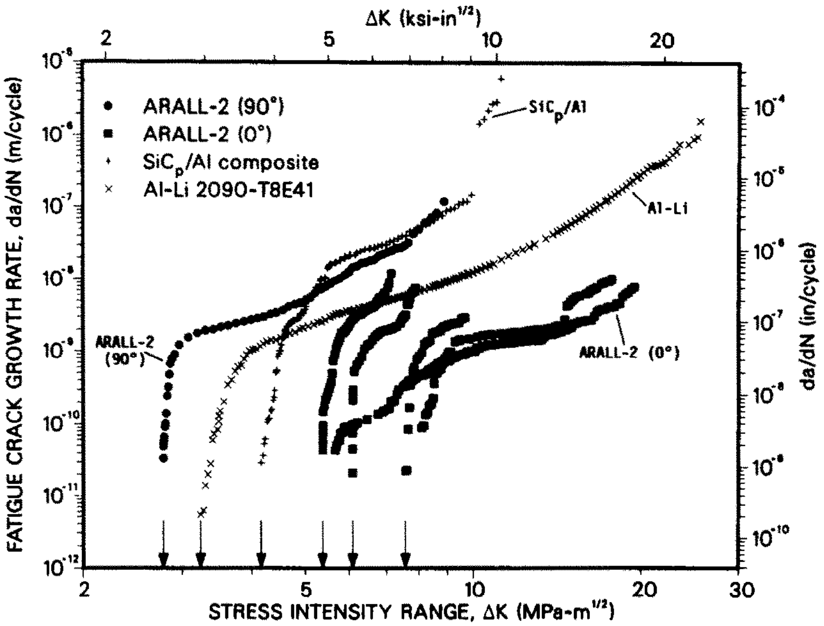

Fig. 13. Comparison of the fatigue crack propagation behavior of ARALL-2 (0° and 90° orientations), as a function of ΔK at $R = 0.1$, with other advanced aluminum alloys, namely aluminum–lithium alloy 2090-T8E41 and SiC-particulate reinforced P/M Al–9%Zn–3%Mg–$2\frac{1}{2}$%Cu (ALCOA MB78) metal-matrix composite. Data for 2090 and SiC_p/Al composite taken from refs [30] and [18], respectively.

ΔK levels are not plotted in Fig. 12 as they involve macroscopic crack bifurcation and thus are not amenable to this simple analysis.)

Comparison with advanced aluminum alloys

From the perspective of high-performance applications, ARALL Laminates must compete with other advanced aluminum alloys, and in particular with aluminum–lithium alloys and metal-matrix composites. A comparison of the fatigue crack growth performance of these materials at ambient temperatures is shown in Fig. 13, based on the current ARALL-2 data and published results (at $R = 0.1$) for a commercial aluminum–lithium alloy 2090-T8E41[40] and a SiC-particulate reinforced P/M Al–9%Zn–3%Mg–$2\frac{1}{2}$%Cu (ALCOA MB78) alloy[18]. The fatigue crack growth resistance of ARALL-2 in the transverse (90°) orientation is inferior to that of the other alloys; however, in the longitudinal (0°) orientation where cracks propagate perpendicular to the fiber direction, the laminate is superior to the metal-matrix composite, and furthermore shows significantly improved crack growth properties over the aluminum–lithium alloy. Since the 2090-T8E41 alloy may be considered as having (long-crack) fatigue properties superior to most, if not all, high-strength monolithic aluminum alloys (e.g. ref. [41]), the use of ARALL for unidirectionally loaded, fatigue-critical structures provides a clear potential for markedly improved durability and damage-tolerance.

CONCLUSIONS

Based on an experimental study of fatigue crack propagation and crack-tip shielding behavior in a 2024-T351 aluminum-alloy/aramid-fiber epoxy 3/2 laminated composite, ARALL-2 Laminate, the following conclusions can be made:

1. Over the range of growth rates from $\sim 10^{-11}$ to 10^{-5} m/cycle (at $R = 0.1$), rates of fatigue crack propagation in ARALL-2 were found to be far slower than in the constituent matrix alloy 2024-T351 for crack advance perpendicular to the fiber direction (0° or longitudinal orientation); rates parallel to the fiber direction (90° or transverse orientation), conversely, were typically a factor of 4 faster.

2. Whereas differences in the growth-rate behavior between ARALL-2 and monolithic

2024-T351 can be predicted in the transverse (90°) orientation by assuming that the fibers play no role and that the aluminum-alloy layers carry all load, the superior crack-growth resistance of the laminate in the longitudinal (0°) orientation is associated with crack-tip shielding primarily by crack bridging from unbroken aramid fibers in the wake of the crack tip, with smaller contributions from crack closure and bifurcation.

3. The occurrence of crack bridging by unbroken fibers was promoted by controlled delamination, principally along the fiber/epoxy interfaces. Using wake-removal experiments, the length of crack over which the fibers remained unbroken in the wake of the crack tip, i.e. the bridging zone, was found to be between 3 and 5 mm, far larger than shielding zones measured for other mechanisms of shielding.

4. Owing to such extensive shielding from crack bridging, fatigue crack growth rates in the longitudinal (0°) orientation were crack-size and history dependent and showed no unique correlation with the applied stress-intensity range ΔK.

5. A new experimental procedure, involving both electrical-potential and back-face strain compliance monitoring, is presented to enable the measurement of the reduction in effective K_{max} in the fatigue cycle due to crack bridging. Coupled with standard unloading compliance measurements of the increase in effective K_{min} due to crack closure, an effective (near-tip) stress-intensity range, ΔK_{eff}, can be derived which embodies the effect of both crack bridging and closure. When characterized in terms of this local field parameter, longitudinal crack growth rates in ARALL lose their crack-size and history dependence and become a unique function of ΔK_{eff}.

6. Under tension–tension fatigue loading, ARALL-2 Laminates display inferior crack-propagation resistance in the transverse (90°) orientation, and superior fatigue crack-propagation resistance in the longitudinal (0°) orientation, compared to monolithic aluminum–lithium and SiC-particulate reinforced aluminum alloys.

Acknowledgements—This work was supported by the U.S. Air Force Office of Scientific Research under Grant No. AFOSR-87-0158, with Dr A. H. Rosenstein as contract monitor. The authors would like to thank Alcoa, specifically Dr L. N. Mueller, for providing the ARALL-2 material, R. H. Dauskardt for several helpful discussions, and Leela Gill and Hiro Hayashigatani for experimental assistance.

REFERENCES

[1] J. Schijve and L. B. Vogelesang, Development of ARALL, a new material for aircraft structures. Memorandum M-434, Delft Univ. of Technology, Dept of Aerospace Engineering (September 1982).

[2] L. B. Vogelesang and J. W. Gunnink, ARALL, a material for the next generation of aircraft. A state of art. Report LR-400, Delft Univ. of Technology, Dept of Aerospace Engineering (August 1983).

[3] L. N. Mueller, J. L. Prohaska and J. W. Davis: ARALL (Aramid Aluminum Laminates): Introduction of a new composite material. *Proc. AIAA Aerospace Engng Conf.*, AIAA, Los Angeles, CA (1985).

[4] L. B. Vogelesang and J. W. Gunnick, ARALL: a materials challenge for the next generation of aircraft. *Mater. Design.* **7,** 2 (1986).

[5] R. Marissen, Flight simulation behavior of aramid reinforced aluminum laminates (ARALL). *Engng Fracture Mech.* **19,** 261–277 (1984).

[6] R. Marissen, K. H. Trautmann, J. Foth and H. Nowack, Microcrack growth in aramid reinforced aluminum laminates (ARALL), *Fatigue 84, Proc. 2nd Int. Conf. on Fatigue and Fatigue Thresholds* (Edited by C. J. Beevers), vol. II, pp. 1081–1091. EMAS Ltd, Warley, U.K. (1984).

[7] R. Marissen, Fatigue crack growth in aramid reinforced aluminum laminates (ARALL), mechanisms and predictions. Report DFVLR-FB-84-37, DFVLR, Institut fur Werkstoff-Forschung (1984).

[8] R. Marissen, Fatigue mechanisms in ARALL, a fatigue resistant hybrid aluminum aramid composite material. *Fatigue 87, Proc. 3rd Int. Conf. on Fatigue and Fatigue Thresholds* (Edited by R. O. Ritchie and E. A. Starke), vol. 3, pp. 1271-1279. EMAS Ltd, Warley, U.K. (1987).

[9] D. B. Marshall, B. N. Cox and A. G. Evans, The mechanics of matrix cracking in brittle-matrix fiber composites. *Acta Metall.* **33,** 2013–2021 (1985).

[10] R. J. Bucci, L. N. Mueller, R. W. Schultz and J. L. Prohaska, ARALL laminates—results from a cooperative test program. *Advanced Materials Technology 87, Proc. 32nd Int. SAMPE Symp., Sci. of Adv. Mater. and Proc. Engng*, vol. 32, p. 902 (1987).

[11] R. O. Ritchie and W. Yu, Short crack effects in fatigue: a consequence of crack tip shielding, in *Small Fatigue Cracks* (Edited by R. O. Ritchie and J. Lankford), pp. 167–198. TMS-AIME, Warrendale, PA (1986).

[12] R. O. Ritchie, Crack tip shielding in fatigue, in *Mechanical behavior of materials-V, Proc. 5th Int. ICM Conf.* (Edited by M. G. Yan, S. H. Zhang and Z. M. Zheng), vol. 3. Pergamon Press, Oxford, U.K. (1987).

[13] A. G. Evans, Z. B. Ahmad, D. G. Gilbert and P. W. R. Beaumont, Mechanics of toughening in rubber toughened polymers. *Acta Metall.* **34,** 79–87 (1986).

[14] A. G. Evans and R. M. Cannon, Toughening of brittle solids by martensitic transformations. *Acta Metall.* **34,** 761–800 (1986).

[15] A. G. Evans and K. T. Faber, Crack-growth resistance of microcracking brittle materials. *J. Am. Ceram. Soc.* **67,** 250–260 (1984).
[16] A. R. Rosenfield and B. S. Majumdar, A micromechanical model for cleavage crack reinitiation. *Metall. Trans. A* **18A,** 1053–1059 (1987).
[17] Y.-W. Mai and B. R. Lawn, Crack-interface grain bridging as a fracture resistance mechanism in ceramics. II. Theoretical fracture mechanics model. *J. Am. Ceram. Soc.* **70,** 289–294 (1987).
[18] J.-K. Shang, W. Yu and R. O. Ritchie, Role of silicon carbide particles in fatigue crack growth in SiC particulate-reinforced aluminum alloy composites. *Mater. Sci. Engng.* In press (1988).
[19] S. Suresh and R. O. Ritchie, Near-threshold fatigue crack propagation: a perspective on the role of crack closure, in *Fatigue Crack Growth Threshold Concepts* (Edited by D. L. Davidson and S. Suresh), pp. 227–261. TMS-AIME, Warrendale, PA (1984).
[20] S. Suresh and R. O. Ritchie, The propagation of short fatigue cracks. *Int. Metals Rev.* **29,** 445–476 (1981).
[21] J. Lankford, Influence of microstructure in the growth of small fatigue cracks. *Fatigue Fract. Engng Mater. Struct.* **8,** 161–175 (1985).
[22] J. W. Hutchinson, Crack tip shielding by micro-cracking in brittle solids. *Acta Metall.* **35,** 1605–1619 (1987).
[23] W. Elber, The significance of crack closure, in *Damage Tolerance in Aircraft Structures*, 230–242. American Society for Testing and Materials, Philadelphia, PA (1971).
[24] J. E. Allison, On the measurement of crack closure during fatigue crack growth, in *Fracture Mechanics 18th Symposium* (Edited by R. P. Read and D. T. Reed), pp. 913–933. American Society for Testing and Materials, Philadelphia, PA (1988).
[25] M. A. Gregory, ARALL® 2 Laminates. Preliminary technical information. Alcoa Technical Report, Aluminum Company of America, Alcoa Center, PA (1987).
[26] R. J. Bucci, L. N. Mueller, L. B. Vogelesang and J. W. Gunnick, ARALL Laminates: properties and design update, in *Materials—Pathway to the Future, Proc. 33rd Int. SAMPE Symp.*, Anaheim, CA (1988); also Alcoa Technical Report No. 57-87-26, Alcoa, Alcoa Center, PA (1987).
[27] H. Tada, P. C. Paris and G. R. Irwin, *The Stress Analysis of Cracks Handbook*, 2nd edn. Paris Productions/Del Research Corp., St. Louis, MO (1985).
[28] F. E. H. M. Smulders and G. H. J. J. Roebroeks, Mechanism of prepreg failure under $R = 0$ fatigue loading in ARALL laminate. Technical report, Delft University of Technology, Dept of Aerospace Engineering (1987).
[29] K. Minakawa, J. C. Newman and A. J. McEvily, A critical study of the crack closure effect on near-threshold fatigue crack growth. *Fatigue Engng Mater. Struct.* **6,** 359–365 (1983).
[30] E. Zaiken and R. O. Ritchie, On the development of crack closure and the threshold condition for short and long fatigue cracks in 7150 aluminum alloy. *Metall. Trans.* **16A,** 1467–1477 (1985).
[31] S. Suresh, D. M. Parks and R. O. Ritchie, Crack tip oxide formation and its influence on fatigue thresholds, in *Fatigue Thresholds, Proc. 1st Int. Conf. on Fatigue Thresholds* (Edited by J. Bäcklund, A. F. Blom and C. J. Beevers), vol. I, pp. 391–408. EMAS Ltd, Warley, U.K. (1982).
[32] S. Suresh and R. O. Ritchie, Some considerations on the modelling of oxide-induced fatigue crack closure using solutions for a rigid wedge inside a linear elastic crack. *Scripta Metall.* **17,** 575–580 (1983).
[33] J.-L. Tzou, C. H. Hseuh, A. G. Evans and R. O. Ritchie, Fatigue crack propagation in oil environments—II. A model for crack closure induced by viscous fluids. *Acta Metall.* **33,** 117–127 (1985).
[34] R. D. Carter, E. W. Lee, E. A. Starke and C. J. Beevers, The effect of microstructure and environment on fatigue crack closure of 7475 aluminum alloy. *Metall. Trans.* **15A,** 555–563 (1984).
[35] W. F. Deans and C. E. Richards, A simple and sensitive method of monitoring crack length and load in compact fracture mechanics specimens using strain gauges. *J. Test. Eval.* **7,** 147–154 (1979).
[36] C. E. Richards and W. F. Deans, The measurement of crack length and load using strain gauges, in *The Measurement of Crack Length and Shape during Fracture and Fatigue* (Edited by C. J. Beevers), pp. 28–68. EMAS Ltd, Warley, U.K. (1980).
[37] D. C. Maxwell, Strain-based compliance method for determining crack length for a C(T) specimen. Materials Laboratory, Air Force Wright Aeronautical Laboratories, Report No. AFWAL-TR-87-4046, Wright-Patterson Air Force Base, Dayton, OH (1987).
[38] P. K. Liaw, H. R. Hartmann and W. A. Logsdon, A new transducer to monitor fatigue crack propagation. *J. Test. Eval.* **11,** 202–207 (1983).
[39] R. H. Dauskardt, W. Yu and R. O. Ritchie, Fatigue crack propagation in a transformation-toughened zirconia ceramic. *J. Am. Ceram. Soc.* **70,** C248–252 (1987).
[40] K. T. Venkateswara Rao, W. Yu and R. O. Ritchie, Fatigue crack propagation in aluminum–lithium alloy 2090: Part I. Long crack behavior. *Metall. Trans.* **19A,** 549–561 (1988).
[41] K. T. Venkateswara Rao, W. Yu and R. O. Ritchie, On the behavior of small fatigue cracks in commercial aluminum–lithium alloys. *Engng Fracture Mech.* **31,** 623–635 (1988).

(*Received 19 January 1988*)